Calorie restriction enhances cell adaptation to hypoxia through Sirt1-dependent mitochondrial autophagy in mouse aged kidney

Shinji Kume,[1,2] Takashi Uzu,[1] Kihachiro Horiike,[2] Masami Chin-Kanasaki,[1] Keiji Isshiki,[1] Shin-ichi Araki,[1] Toshiro Sugimoto,[1] Masakazu Haneda,[3] Atsunori Kashiwagi,[1] and Daisuke Koya[4]

[1]Department of Medicine and [2]Department of Biochemistry and Molecular Biology, Shiga University of Medical Science, Japan. [3]Department of Medicine, Asahikawa Medical College, Japan. [4]Division of Endocrinology and Metabolism, Kanazawa Medical University, Kahoku-Gun, Japan.

Mitochondrial oxidative damage is a basic mechanism of aging, and multiple studies demonstrate that this process is attenuated by calorie restriction (CR). However, the molecular mechanism that underlies the beneficial effect of CR on mitochondrial dysfunction is unclear. Here, we investigated in mice the mechanisms underlying CR-mediated protection against hypoxia in aged kidney, with a special focus on the role of the NAD-dependent deacetylase sirtuin 1 (Sirt1), which is linked to CR-related longevity in model organisms, on mitochondrial autophagy. Adult-onset and long-term CR in mice promoted increased Sirt1 expression in aged kidney and attenuated hypoxia-associated mitochondrial and renal damage by enhancing BCL2/adenovirus E1B 19-kDa interacting protein 3–dependent (Bnip3-dependent) autophagy. Culture of primary renal proximal tubular cells (PTCs) in serum from CR mice promoted Sirt1-mediated forkhead box O3 (Foxo3) deacetylation. This activity was essential for expression of Bnip3 and p27Kip1 and for subsequent autophagy and cell survival of PTCs under hypoxia. Furthermore, the kidneys of aged *Sirt1*$^{+/-}$ mice were resistant to CR-mediated improvement in the accumulation of damaged mitochondria under hypoxia. These data highlight the role of the Sirt1-Foxo3 axis in cellular adaptation to hypoxia, delineate a molecular mechanism of the CR-mediated antiaging effect, and could potentially direct the design of new therapies for age- and hypoxia-related tissue damage.

Introduction

Increasing age causes progressive postmaturational deterioration of tissues and organs, leading to impairment of tissue functioning, increased vulnerability to challenges, and death. The kidney is a typical target organ of age-associated tissue damage, and the increased incidence of chronic kidney disease (CKD) in the elderly is a health problem worldwide (1–3). However, there is little or no information on the mechanisms underlying age-associated kidney damage. Thus, studies designed to determine such molecular mechanisms could help formulate interventions that delay the onset and/or progression of CKD in elderly patients.

Among the several proposed theories on the pathogenesis of age-associated tissue damage, the mitochondrial ROS theory provides the basic mechanism of age-associated tissue dysfunction (4, 5): that age-dependent alteration in mitochondrial DNA (mtDNA) plays a fundamental role in the age-associated increase in ROS and subsequent tissue damage (6, 7). Further evidence linking alterations in mtDNA with progressive age-dependent tissue dysfunction can be found in individuals with mitochondrial genetic diseases and mice with deletion mutation of mtDNA, which display a phenotype that resembles premature aging, including kidney dysfunction (8, 9). Hypoxia is the cause of age-associated mitochondrial dysfunction (10) and is involved in age-dependent tissue damage affecting the brain (11), heart (12), and kidney (13). Furthermore, hypoxia modulates various cellular processes, such as apoptosis, cell cycle, autophagy, and glucose metabolism (14, 15). Elderly individuals suffer impairment of adaptation to systemic hypoxemia (16, 17); however, the molecular changes involved in age-associated cellular maladaptation to hypoxia are poorly understood.

Calorie restriction (CR) has various beneficial effects on health, including lifespan prolongation (18, 19). One mechanism of the beneficial effects of CR is attenuation of mitochondrial dysfunction in various pathological conditions (20, 21). Moreover, CR is suggested to affect cell adaptation to hypoxia (22), although the molecular mechanism of this effect remains elusive. In this context, uncovering the mechanism underlying CR-mediated attenuation of age-associated cellular and mitochondrial damage under hypoxia should contribute to the development of new therapies for age-associated tissue damage.

Studies on the mechanisms of CR-related longevity have identified the silent information regulator 2 (Sir2) as a survival factor that prolongs lifespan (23, 24). Sirt1, a mammalian homolog of Sir2, was originally identified as an NAD-dependent histone deacetylase (25). Recent studies have shown that Sirt1 is involved in the regulation of a wide variety of cellular processes, ranging from stress response, cell cycle, metabolism, and apoptosis in response to the cellular energy and redox status, through its deacetylase activity for more than 2 dozen known substrates (26). Thus, although Sirt1 is linked to CR-related longevity in model organisms (23, 24), the mechanism by which it extends lifespan in mammals and its role in age- or hypoxia-associated tissue damage remains unclear.

In the present study, we examined the mechanism of CR-related mitochondrial and cellular protection against hypoxia in aged mouse

Conflict of interest: The authors have declared that no conflict of interest exists.
Citation for this article: *J Clin Invest.* 2010;120(4):1043–1055. doi:10.1172/JCI41376.

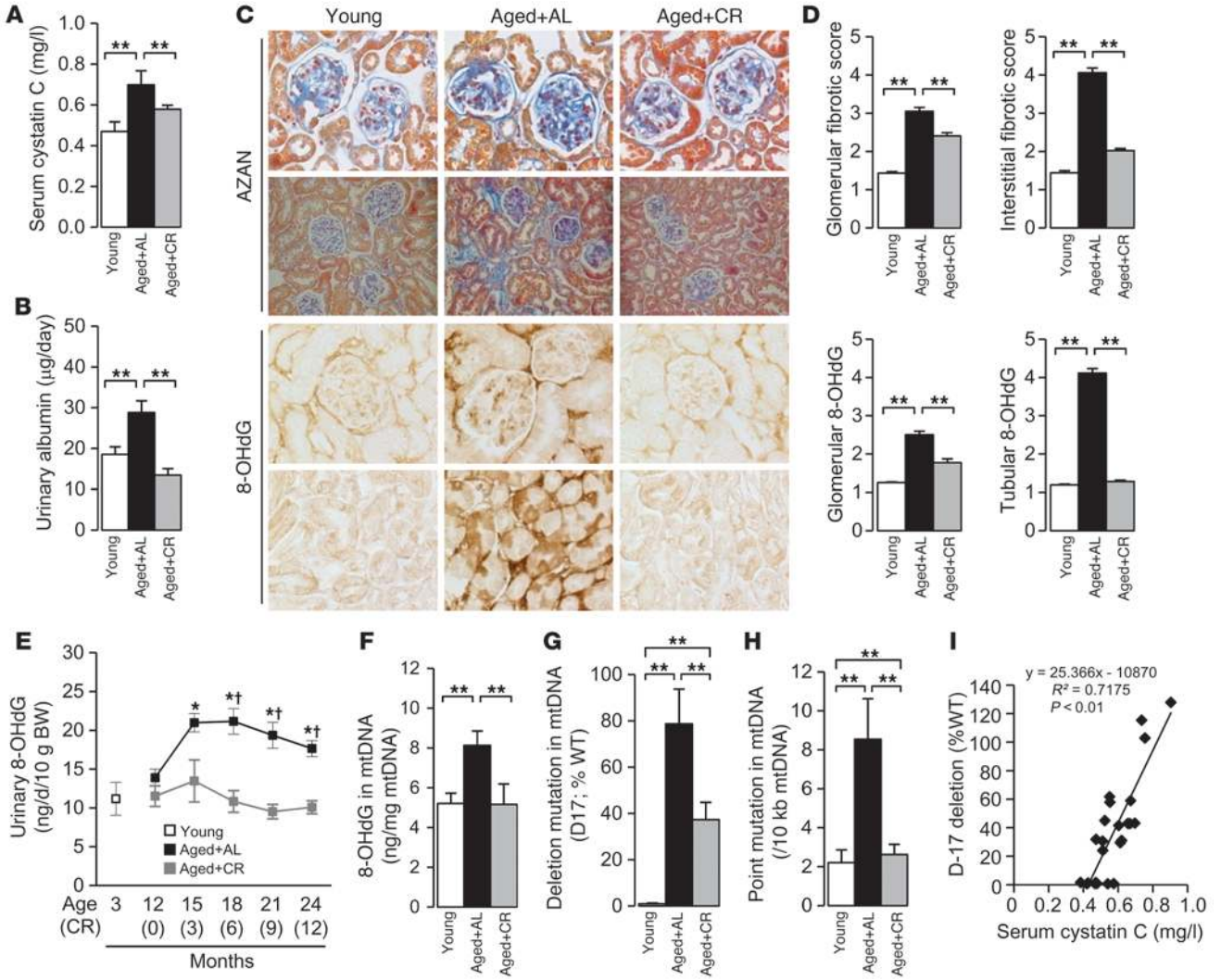

Figure 1

Effect of CR on mitochondrial oxidative damage in aged kidney. Experiments were performed on young mice or on aged mice subjected to AL or 12 months of CR. (**A** and **B**) Serum cystatin C levels (**A**) and 24-hour urinary albumin excretion levels (**B**) at the end of the experimental period. (**C**) Azan-stained and 8-OHdG–immunostained kidney sections. Original magnification, ×200 (Azan, bottom); ×400 (Azan, top, and 8-OHdG). (**D**) Quantitative analyses of Azan and 8-OHdG staining of glomerular and tubulointerstitial lesions. (**E**) Urinary 8-OHdG excretion levels during the observation period. Data are mean ± SEM. *$P < 0.05$ vs. young, †$P < 0.05$ vs. CR at the same time point. (**F**–**H**) 8-OHdG content (**F**), relative proportion of D-17 deletions (as percentage of WT; **G**), and frequencies of point mutations in cytochrome *b* gene (**H**) in mtDNA isolated from the kidney. Data are mean ± SEM. **$P < 0.05$. Each group includes 7–9 mice. (**I**) Correlation between D-17 prevalence and serum cystatin C level.

kidney, with a special focus on the role of Sirt1 on mitochondrial autophagy. The study identified a role for Sirt1 on cell adaptation to hypoxia, which provides what we believe to be a new molecular finding in CR-mediated antiaging effects, and shed light on the design of new therapies for age-related tissue damage including aged kidney.

Results

CR attenuates mitochondrial oxidative damage in aged kidney. First, we investigated whether adult-onset, long-term CR attenuates kidney damage and oxidative stress in aged mice. (Hereafter, unless otherwise indicated, *young* refers to mice 3 months of age and *aged* to mice 24 months of age.) During the 12-month experimental period, 3 aged mice of the ad libitum–fed (AL) group died as a result of malignancy and liver cirrhosis, whereas a single mouse of the CR group died as a result of malignancy (Supplemental Table 1; supplemental material available online with this article; doi:10.1172/JCI41376DS1). Significant differences were noted in various systemic metabolic parameters between the CR and AL mice (Supplemental Table 1). CR significantly inhibited age-associated increases in the renal dysfunction marker serum cystatin C, 24-hour urinary albumin excretion, and fibrotic changes in glomerular and interstitial lesions, with significantly reduced urinary excretion of the oxidative stress marker 8-OHdG (Figure 1, A–E). Significant accumulation of 8-OHdG was observed especially in the cytoplasm of the proximal tubular cells (PTCs) of AL mice, which was significantly attenuated by CR (Figure 1, C and D). In the kidneys of AL mice, accumulation of 8-OHdG in glomeruli was less than that in PTCs (Figure 1, C and D). Age-dependent

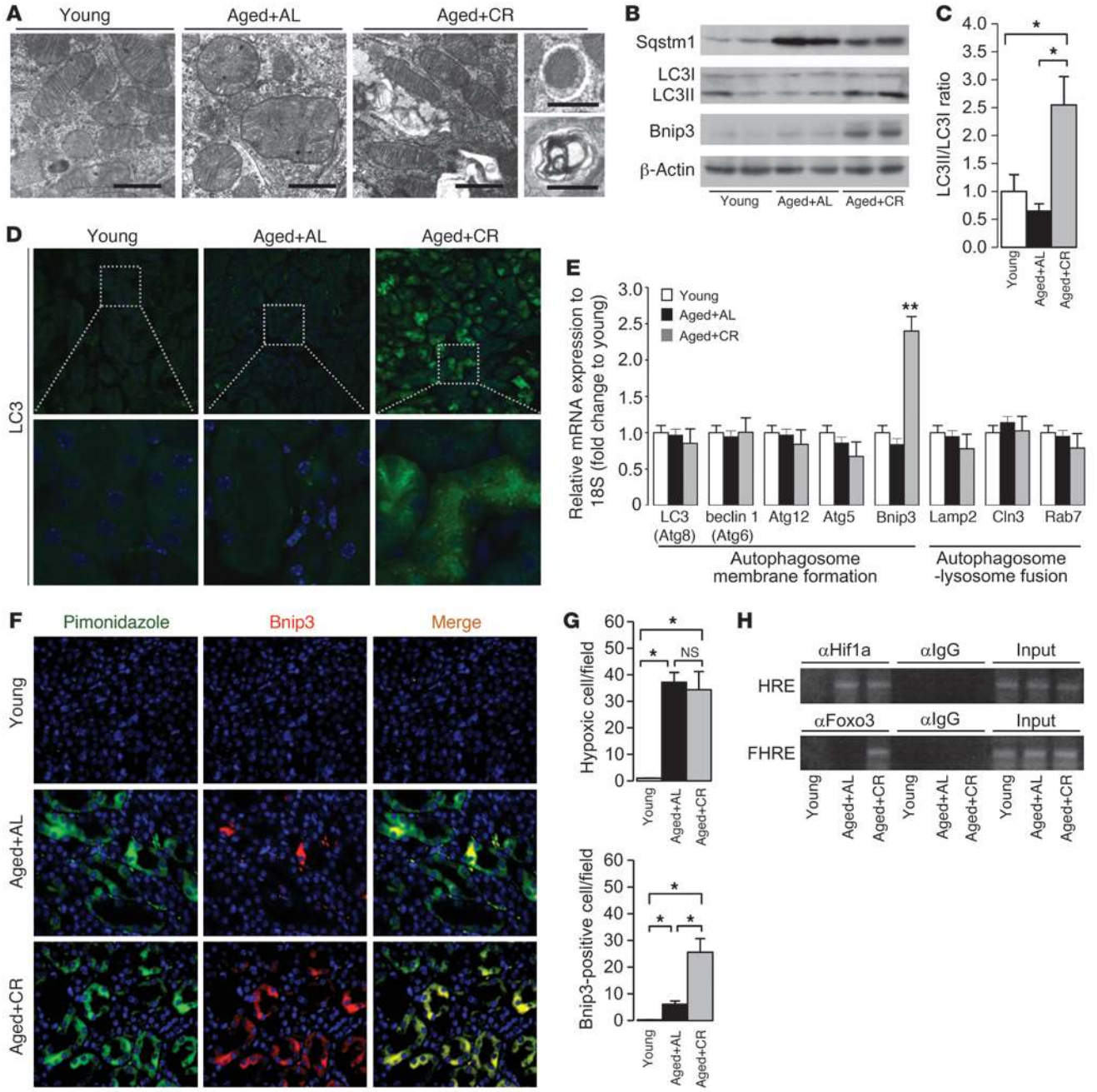

Figure 2

Effect of CR on Bnip3-mediated autophagy in aged kidney. (**A**) EM of representative renal PTCs. Scale bars: 1 μm. (**B**) IB analysis for autophagy-associated molecules. (**C**) Quantitative analysis of band intensity for LC3I and LC3II (ratio of LC3II to LC3I). (**D**) Immunofluorescent study for LC3 protein in the kidney. Original magnification, ×400 (top); ×1,000 (bottom). DAPI staining was performed as counterstaining. (**E**) mRNA expression associated with auto(lyso)phagosomal formation. Data are assessed as the ratio of mRNA expression of each molecule to mRNA expression of 18S ribosomal RNA and expressed as the fold change relative to the mean value of young mice. (**F**) Immunofluorescence study for pimonidazole and Bnip3 in the kidney. Original magnification, ×400. (**G**) Quantitative analysis of hypoxic pimonidazole$^+$ and Bnip3$^+$ cells per field in the kidney. (**H**) ChIP analysis to determine Hif1a and Foxo3 binding to Bnip3 promoter in the kidney samples. HRE, Hif-responsive element; FHRE, forkhead response element. Data are mean ± SEM. *P < 0.05. **P < 0.05 vs. other groups. Each group includes 7–9 mice.

increases in 8-OHdG accumulation as well as the major deletion mutation D-17 and point mutations in mtDNA are markers of age-associated mtDNA oxidative damage (27, 28). The age-associated mtDNA oxidative damages were significantly increased in the kidneys of AL mice and attenuated by CR (Figure 1, F–H). The prevalence of D-17 correlated significantly with serum cystatin C levels (Figure 1I), which suggests that mtDNA oxidative damage is related to age-dependent kidney dysfunction.

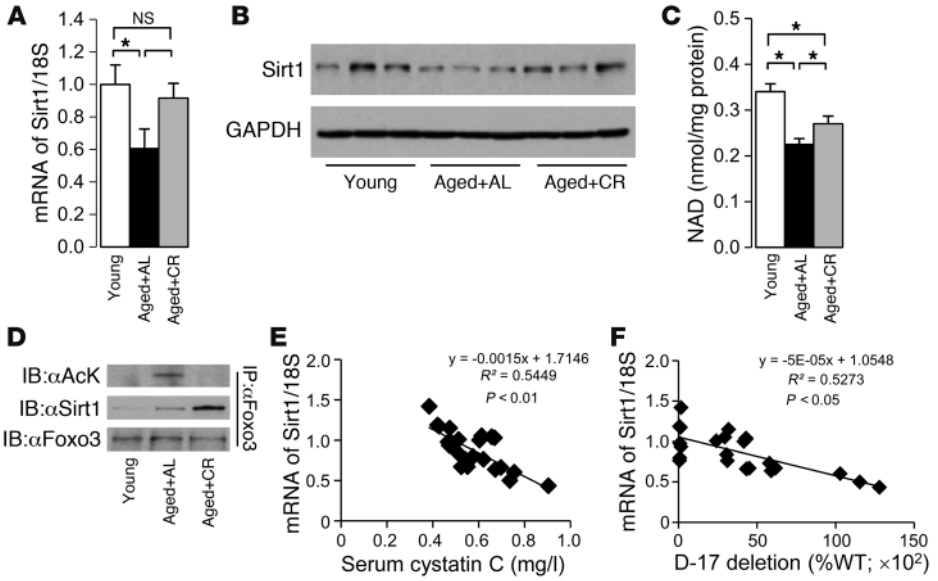

Figure 3
Effect of CR on Sirt1 activity in aged kidney. (**A** and **B**) mRNA (**A**) and protein (**B**) expression levels of Sirt1 in kidney samples. (**C**) NAD contents in kidney samples. (**D**) IP to detect acetylation of Foxo3 and interaction between Sirt1 and Foxo3 in kidney samples. Data are mean ± SEM. *$P < 0.05$. Each group includes 7–9 mice. (**E**) Correlation between Sirt1 mRNA expression level and serum cystatin C level. (**F**) Correlation between Sirt1 mRNA expression level and D-17 prevalence.

CR enhances autophagy in aged kidney. EM analysis showed accumulation of senescent mitochondria in PTCs of AL mice, which exhibited swelling and disintegration of cristae (Figure 2A). Under normal circumstances, damaged mitochondria are degraded by autophagy, an intracellular process that allows the degradation of damaged proteins and organelles (29). In contrast to PTCs of AL mice, those of CR mice showed normal mitochondrial morphology with numerous auto(lyso)phagosomes (Figure 2A). Moreover, kidneys of AL mice contained higher levels of sequestosome 1 (Sqstm1; Figure 2B), a marker for in vivo impaired autophagy (30, 31). Lipidation of microtubule-associated protein 1 light chain 3 alpha (LC3), as assessed by the ratio of LC3I to LC3II conversion, as well as LC3 dots, which are known markers of enhanced autophagy (32, 33), were lower in AL mice than in CR mice (Figure 2, B–D). Thus, impaired autophagy might cause age-dependent mitochondrial oxidative damage in the kidney, and enhancement of autophagy could explain the CR-mediated mitochondrial protection.

CR enhances hypoxia-induced expression of BCL2/adenovirus E1B 19-kDa interacting protein 3 in aged kidney. We next analyzed the mRNA expression levels of various molecules involved in auto(lyso)phagosome formation (Figure 2E). Overexpression of BCL2/adenovirus E1B 19-kDa interacting protein 3 (Bnip3) mRNA was detected in CR mice (Figure 2E), and this was confirmed by IB (Figure 2B). Because Bnip3 is an initiator of hypoxia-induced autophagy (15, 34, 35), we examined the state of hypoxia and Bnip3 expression in the kidney. Pimonidazole$^+$ hypoxic cells were observed in PTCs of both AL and CR mice (Figure 2, F and G). Bnip3 expression was significantly enhanced in hypoxia-positive PTCs of CR mice, but it was less noted in AL mice (Figure 2, F and G). Bnip3 expression is positively regulated by certain transcriptional factors, including hypoxia-inducible factor 1 alpha (Hif1a) and forkhead box O3 (Foxo3) (15, 36). Chromatin IP (ChIP) indicated that Hif1a bound to Bnip3 promoter in the kidneys of both AL and CR mice, but Foxo3 bound to Bnip3 promoter only in CR mice (Figure 2H). These results suggest that Foxo3-mediated Bnip3 overexpression should be a molecular target for CR-mediated enhancement of hypoxia-induced autophagy in the aged kidney.

CR enhances Sirt1 activity in aged kidney. Because Foxo3 transcriptional activity is regulated by Sirt1 under certain conditions (37), we checked Sirt1 activity and its interaction with Foxo3. The mRNA and protein expression levels of Sirt1 were significantly decreased in the kidneys of AL mice and enhanced by long-term CR (Figure 3, A and B). NAD content in AL mice significantly decreased compared with that of young mice, but this decrease was attenuated by CR (Figure 3C). IP analysis revealed that Sirt1 interacted with and deacetylated Foxo3 in the kidney of CR mice, but not in AL mice (Figure 3D). Thus, Sirt1 activity was decreased in the aged kidney and enhanced by long-term CR. Furthermore, Sirt1 mRNA expression levels correlated negatively with serum cystatin C levels and prevalence of D-17 (Figure 3, E and F), which suggests that Sirt1 is associated with age-associated kidney dysfunction and mitochondrial damage.

Foxo3 is essential for CR-mediated enhancement of hypoxia-induced Bnip3 expression and autophagy. To investigate whether CR-dependent enhancement of hypoxia-induced Bnip3 expression and autophagy is reproducible in vitro, PTCs were incubated with serum from CR or AL rodents (20, 38, 39), and then exposed to hypoxia (1% O_2) for 24 hours. We reproduced a clear enhancement of hypoxia-induced Bnip3 expression as well as autophagy, as determined by LC3II formation and LC3 dots, in CR serum compared with AL serum (Figure 4, A–C). We confirmed that hypoxia failed to induce autophagy in Bnip3-knockdown cells (Supplemental Figure 1), which suggests that Bnip3 is essential for hypoxia-induced autophagy in PTCs. The siRNA for Foxo3 significantly inhibited CR-mediated enhancement of hypoxia-induced Bnip3 expression and autophagy (Figure 4, A–C). However, Foxo3 deficiency failed to inhibit hypoxia-induced autophagy in Bnip3-overexpressing PTCs under CR serum (Figure 4, D–F), which suggests that Foxo3 regulates hypoxia-induced autophagy through Bnip3 overexpression in CR serum.

Sirt1 is essential for CR-mediated enhancement of hypoxia-induced Bnip3 expression and autophagy. Retrovirally mediated Sirt1 knockdown significantly inhibited CR-mediated enhancement of hypoxia-induced Bnip3 expression and autophagy (Figure 5, A–C). Dominant-negative Sirt1 (H355A) lacking deacetylase activity inhibited hypoxia-induced autophagy under CR serum, whereas it failed to inhibit autophagy in Bnip3-overexpressing PTCs (Figure 5, D–F). Furthermore, Sirt1 overexpression did not affect Bnip3 knock-

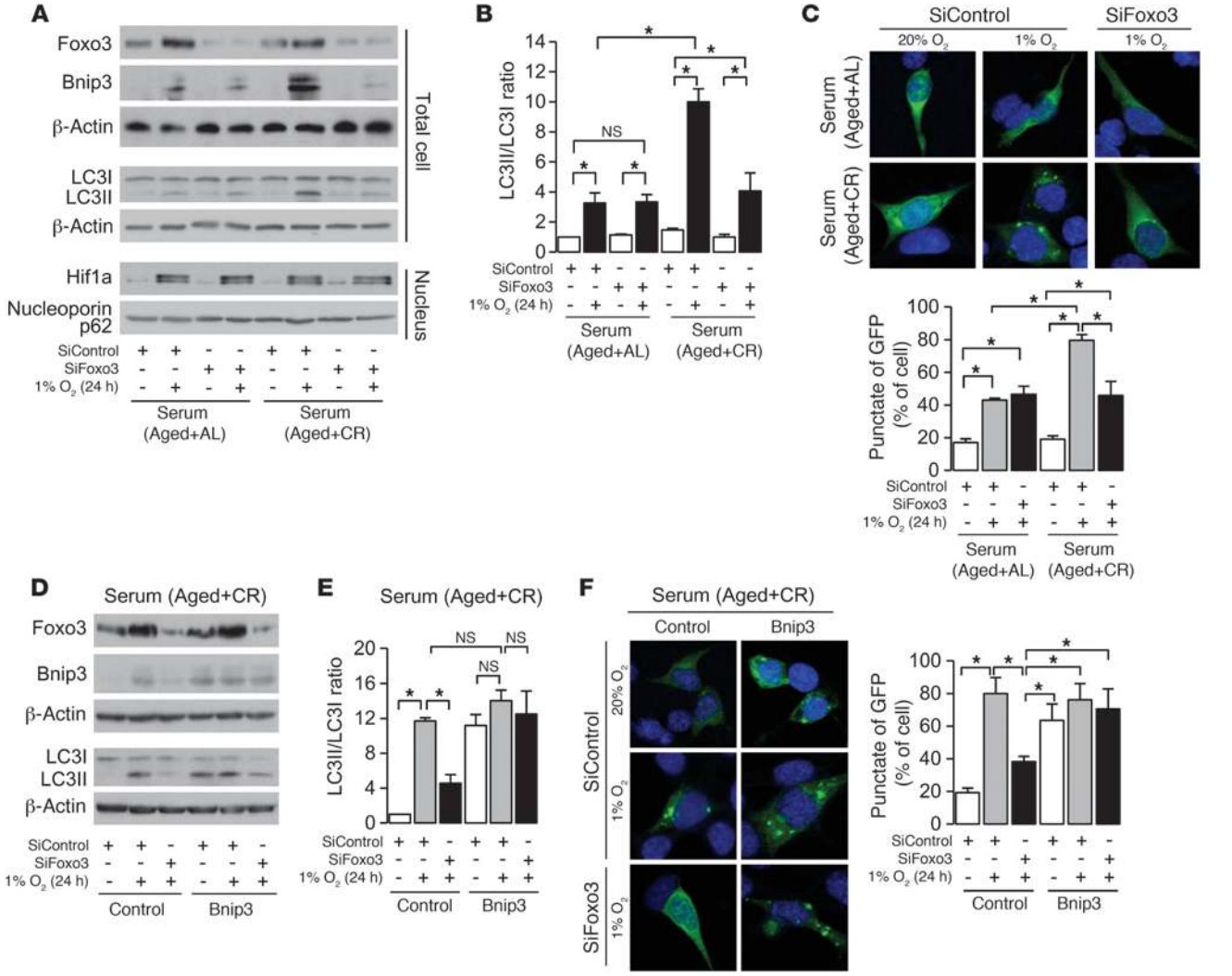

Figure 4

Involvement of Foxo3 on CR-mediated enhancement of autophagy under hypoxia. (**A**) Expression of Foxo3, autophagy-associated molecules, and nuclear Hif1a under hypoxia (1% O_2, 24 hours) in cells transfected with siRNA control or siRNA for Foxo3 under AL or CR serum. To detect LC3I and LC3II bands, cells were preincubated with lysosomal inhibitor (E64d and pepstatin A). (**B**) Quantitative analysis of the ratio of LC3II to LC3I ($n = 4$). (**C**) Hypoxia-induced autophagy in cells transfected with siRNA control or siRNA for Foxo3 in AL or CR serum. Autophagy was detected as dot spot of GFP-LC3 protein. Original magnification, ×400. Bottom: Percentage of GFP$^+$ cells with punctate GFP-LC3 fluorescence. (**D**) Expression of Foxo3 and autophagy-associated molecules under hypoxia in retrovirally mediated Bnip3-overexpressing cells transfected with siRNA control or siRNA for Foxo3 in CR serum. To detect LC3I and LC3II bands, cells were preincubated as in **A**. (**E**) Quantitative analysis of the ratio of LC3II to LC3I ($n = 4$). (**F**) Hypoxia-induced autophagy in Bnip3-overexpressing cultured cells transfected with siRNA control or siRNA for Foxo3 in CR serum. Original magnification, ×400. Right: Percentage of GFP$^+$ cells with punctate GFP-LC3 fluorescence. Data are mean ± SEM. *$P < 0.05$.

down–mediated inhibition of autophagy (Supplemental Figure 1), which suggests that Sirt1 positively regulates CR-mediated enhancement of hypoxia-induced autophagy upstream of Bnip3.

PI3K and Sirt1 regulate Foxo3 activity in the Bnip3 promoter. Since nuclear translocation of Foxo3 and its subsequent transcriptional activity are negatively regulated by PI3K-Akt–mediated phosphorylation (40), we next examined the role of PI3K and Sirt1 on Foxo3-mediated enhancement of hypoxia-induced Bnip3 expression in AL and CR serum. At the early stage of hypoxia (6 hours), Bnip3 expression was not detected in AL serum, whereas it was enhanced in CR serum (Figure 6A). At this stage, phosphorylated Foxo3 in AL serum showed cytoplasmic localization, and dephosphorylated Foxo3 in CR serum exhibited nuclear distribution (Figure 6, B and C). The PI3K inhibitor LY294002 in AL serum reversed phosphorylation of Foxo3 and enhanced its nuclear translocation (Figure 6, B and C). Because Sirt1 was localized in the nucleus in CR and AL serum (Figure 6B), we next investigated whether nuclear-translocated Foxo3 interacts with Sirt1. In AL serum, Foxo3 failed to interact with Sirt1 and was markedly acetylated even when it was translocated into the nucleus by LY294002 (Figure 6D). In contrast, under CR serum, nuclear Foxo3 interacted with Sirt1 and was deacetylated (Figure 6D). ChIP and IB revealed that acetylated

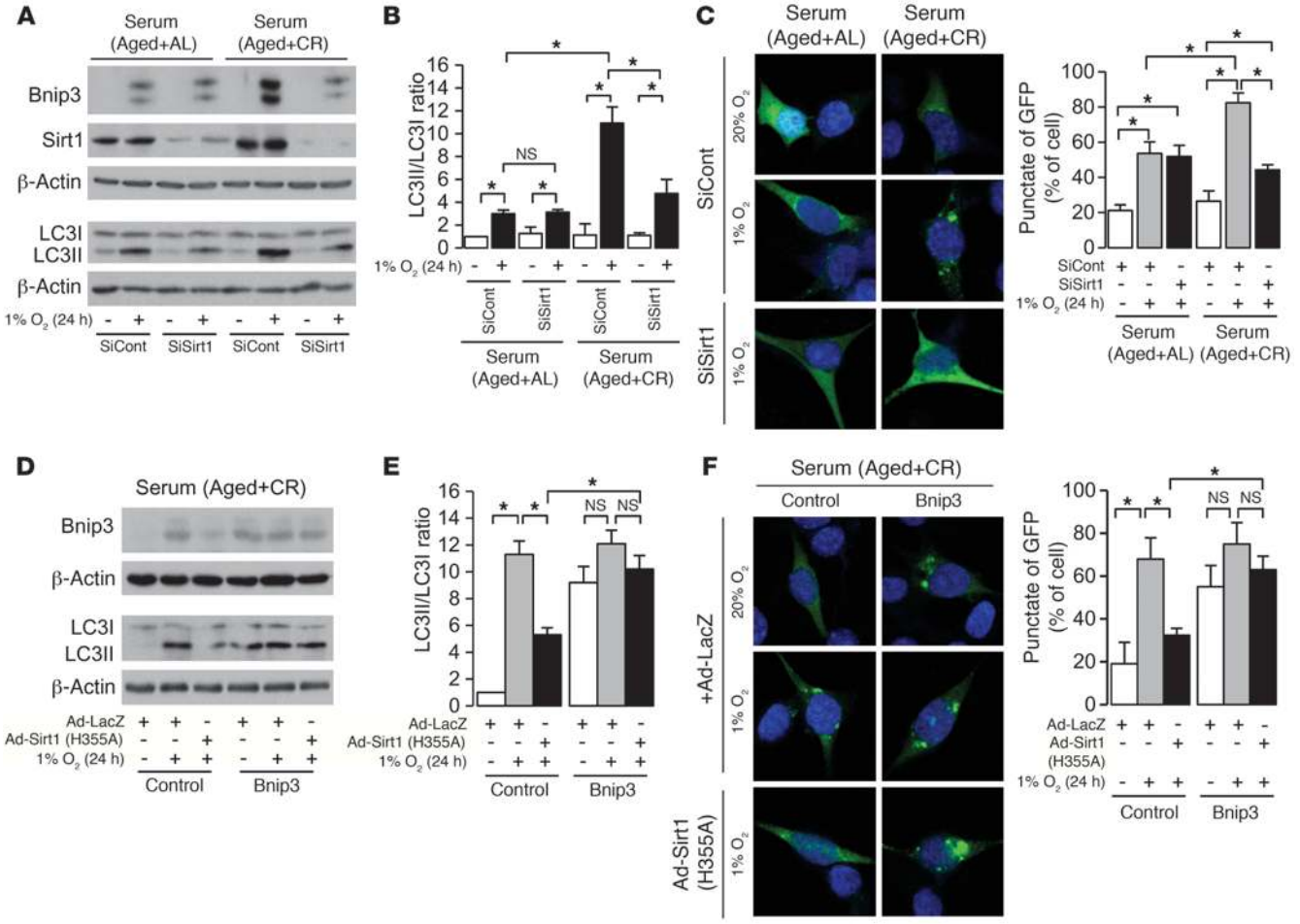

Figure 5

Involvement of Sirt1 in CR-mediated enhancement of autophagy under hypoxia. (**A**) Bnip3 and Sirt1 expression and LC3II formation in retrovirally mediated Sirt1-knockdown cells under hypoxia (1% O_2, 24 hours) in AL and CR serum conditions. To detect LC3I and LC3II bands, cells were preincubated with lysosomal inhibitor (E64d and pepstatin A). (**B**) Quantitative analysis of the ratio of LC3II to LC3I ($n = 4$). (**C**) Hypoxia-induced autophagy in Sirt1-knockdown cells under AL and CR serum conditions. Original magnification, ×400. Right: Percentage of GFP$^+$ cells with punctate GFP-LC3 fluorescence. (**D**) Expression of Bnip3 and LCII formation under hypoxia in retrovirally mediated Bnip3-overexpressing cells infected with either adenoviral mutated Sirt1 (H355A) or LacZ in CR serum. To detect LC3I and LC3II bands, cells were preincubated as in **A**. (**E**) Quantitative analysis of the ratio of LC3II to LC3I ($n = 4$). (**F**) Hypoxia-induced autophagy in retrovirally mediated Bnip3-overexpressing cells infected with either adenoviral mutated Sirt1 (H355A) or LacZ in CR serum. Original magnification, ×400. Right: Percentage of GFP$^+$ cells with punctate GFP-LC3 fluorescence. Data are mean ± SEM. *$P < 0.05$.

Foxo3 in AL serum failed to bind to Bnip3 promoter or enhance Bnip3 expression, whereas deacetylated Foxo3 in CR serum bound to Bnip3 promoter and subsequently enhanced Bnip3 expression under hypoxia (Figure 6, C and E). These conditions did not affect hypoxia-mediated Hif1a expression (Figure 6C).

PI3K and Sirt1 regulate Foxo3-mediated cell adaptation to hypoxia. Foxo3 is also recognized as a cell cycle regulator (G_1 arrest) through p27Kip1 expression (41) and as a proapoptotic factor through Bim expression (37, 42) in response to certain stress conditions. At the late phase (12–24 hours), hypoxia caused apoptosis in AL serum, as determined by cleavage of both poly(ADP-ribose) polymerase (PARP) and caspase 3 (Figure 6A). In contrast, hypoxia in CR serum enhanced p27Kip1 expression as well as autophagy with Bnip3 overexpression (Figure 6A). Thus, we next examined the role of interaction among PI3K, Sirt1, and Foxo3 on p27Kip1 expression, autophagy, and apoptosis in the late phase (24 hours) of hypoxia. Prolonged hypoxia in AL serum partially translocated Foxo3 to the nucleus, and this effect was blocked by N-acetyl-cysteine (NAC), an antioxidant molecule (Figure 7, A and B). NAC also inhibited hypoxia-mediated apoptosis in AL serum (Figure 7B). In contrast, LY294002 increased Foxo3 nuclear translocation and apoptosis (Figure 7, A and B). These results suggest that oxidative stress–mediated nuclear translocation of Foxo3 causes apoptosis under hypoxia in AL serum, which is inhibited by PI3K. In CR serum, Foxo3 was localized in the nucleus under both normoxia and hypoxia (Figure 7, A and B), and Bnip3-mediated autophagy was enhanced under hypoxia (Figure 7, B and C).

Similar to the results of early phase, nuclear Foxo3 failed to interact with Sirt1 and was markedly acetylated in AL serum, whereas it interacted with Sirt1 and was deacetylated in CR serum (Figure 7D). ChIP and IB showed that acetylated Foxo3 in AL serum failed to bind to both Bnip3 and p27Kip1 promoters, and bound to Bim

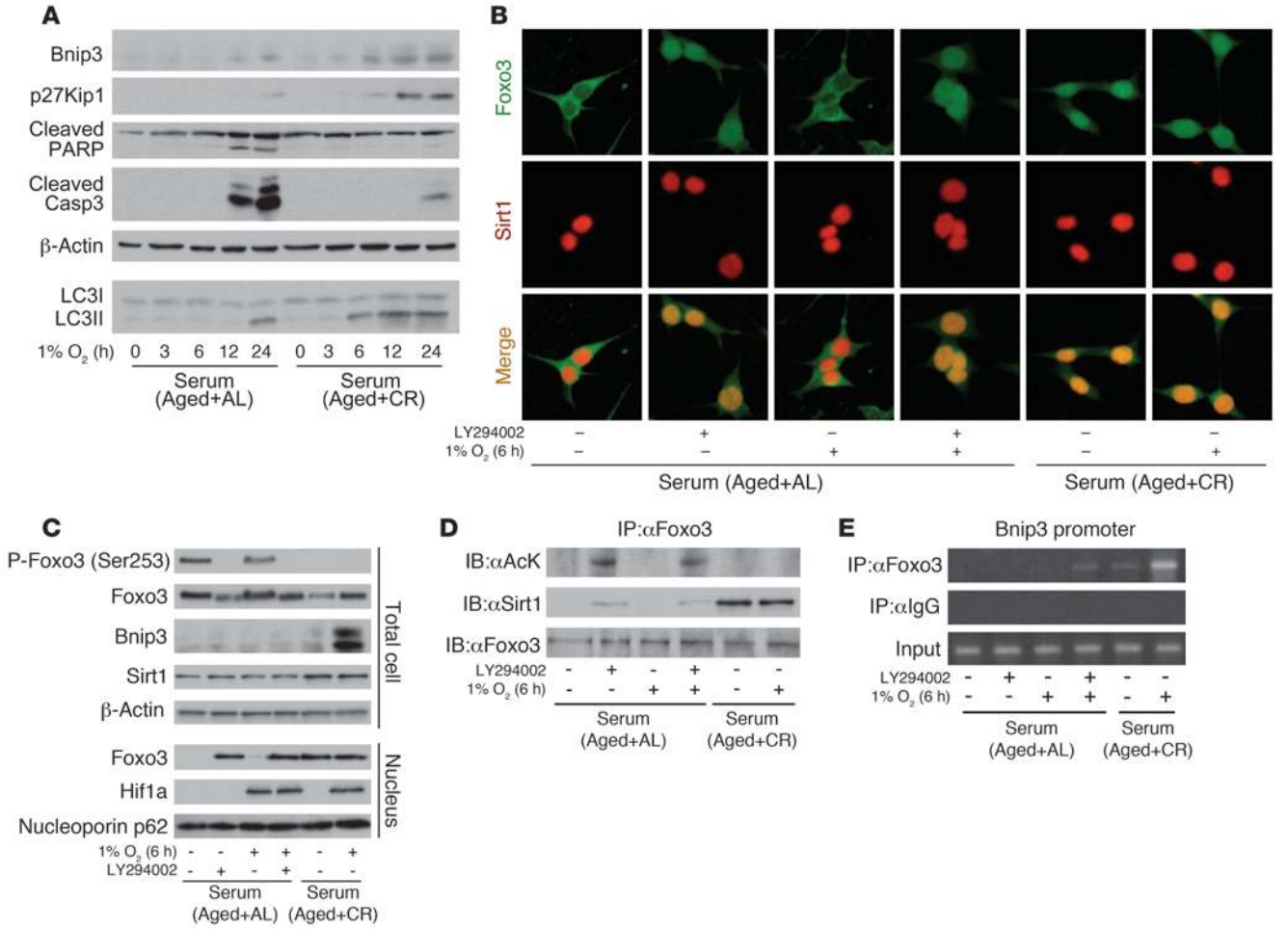

Figure 6

Involvement of PI3K and Sirt1 in Foxo3-mediated Bnip3 expression at early phase of hypoxia. (**A**) IB for Bnip3, p27Kip1, cleaved PARP, and cleaved caspase 3 expression and LC3II formation at the indicated time points under hypoxia (1% O_2) in AL and CR serum. To detect LC3I and LC3II bands, cells were preincubated with lysosomal inhibitor (E64d and pepstatin A). (**B**) Immunostaining showing localization of Foxo3 and Sirt1 at early phase of hypoxia (1% O_2, 6 hours) under the indicated conditions. Original magnification, ×400. (**C**) Phosphorylation and expression levels of Foxo3, expression levels of Bnip3 and Sirt1, and nuclear expression levels of Foxo3 and Hif1a at early phase of hypoxia. (**D**) Acetylation of Foxo3 and interaction between Sirt1 and Foxo3 at early phase of hypoxia. (**E**) ChIP analysis to determine Foxo3 binding to Bnip3 promoters at early phase of hypoxia. LY294002 was used as PI3K inhibitor at 20 μM.

promoter, in hypoxic PTCs (Figure 7E), which suppressed autophagy and p27Kip1 expression and increased apoptosis (Figure 7, B and C). LY294002 enhanced Foxo3 binding to Bim promoter under AL serum (Figure 7E). In contrast, deacetylated Foxo3 in CR serum bound to Bnip3 and p27Kip1 promoters, but not Bim promoters (Figure 7E), which mediated autophagy and p27Kip1 expression and suppressed apoptosis (Figure 7, B and C).

Retrovirally mediated Sirt1 knockdown in CR serum enhanced hypoxia-induced apoptosis and inhibited p27Kip1 expression and Bnip3-mediated autophagy (Figure 8, A and B). We next examined the mechanisms of these actions. Sirt1 deficiency in CR serum enhanced acetylation of Foxo3 (Figure 8C). Acetylated Foxo3 failed to bind to both Bnip3 and p27Kip1 promoter and bound to Bim promoter (Figure 8D). In contrast, Sirt1 overexpression in AL serum with LY294002 augmented Bnip3-mediated autophagy and p27Kip1 expression, decreased apoptosis (Figure 8, E and F), and increased Foxo3 binding to Bnip3 and p27Kip1 promoter (Figure 8G). Under the same conditions, siRNA for Foxo3 suppressed Sirt1-mediated enhancement of Bnip3-mediated autophagy and p27Kip1 expression (Figure 8, E and F), which suggests that Sirt1 promotes cellular adaptation to hypoxia through the regulation of transcriptional activity of Foxo3 to Bnip3, p27Kip1, and Bim.

CR fails to enhance cell adaptation to hypoxia in aged kidney of Sirt1$^{+/-}$ mice. We provided in vivo evidence for the involvement of Sirt1 in CR-mediated cellular adaptation to hypoxia by using 12-month-old *Sirt1*$^{+/-}$ mice on SV129 background under AL and CR for 6 months. The PTCs of 12-month-old WT mice showed normal mitochondrial morphology and little mitochondrial oxidative damage, together with substantial increases in autophagy and hypoxia-associated Bnip3 expression (Figure 9, A–G). In contrast, *Sirt1*$^{+/-}$ AL mice showed damaged mitochondria, higher levels of urinary 8-OHdG excretion, and higher prevalence of point mutation of mtDNA in the kidney; additionally, autophagy and Bnip3 expression in the hypoxic PTCs of *Sirt1*$^{+/-}$ AL mice were significantly

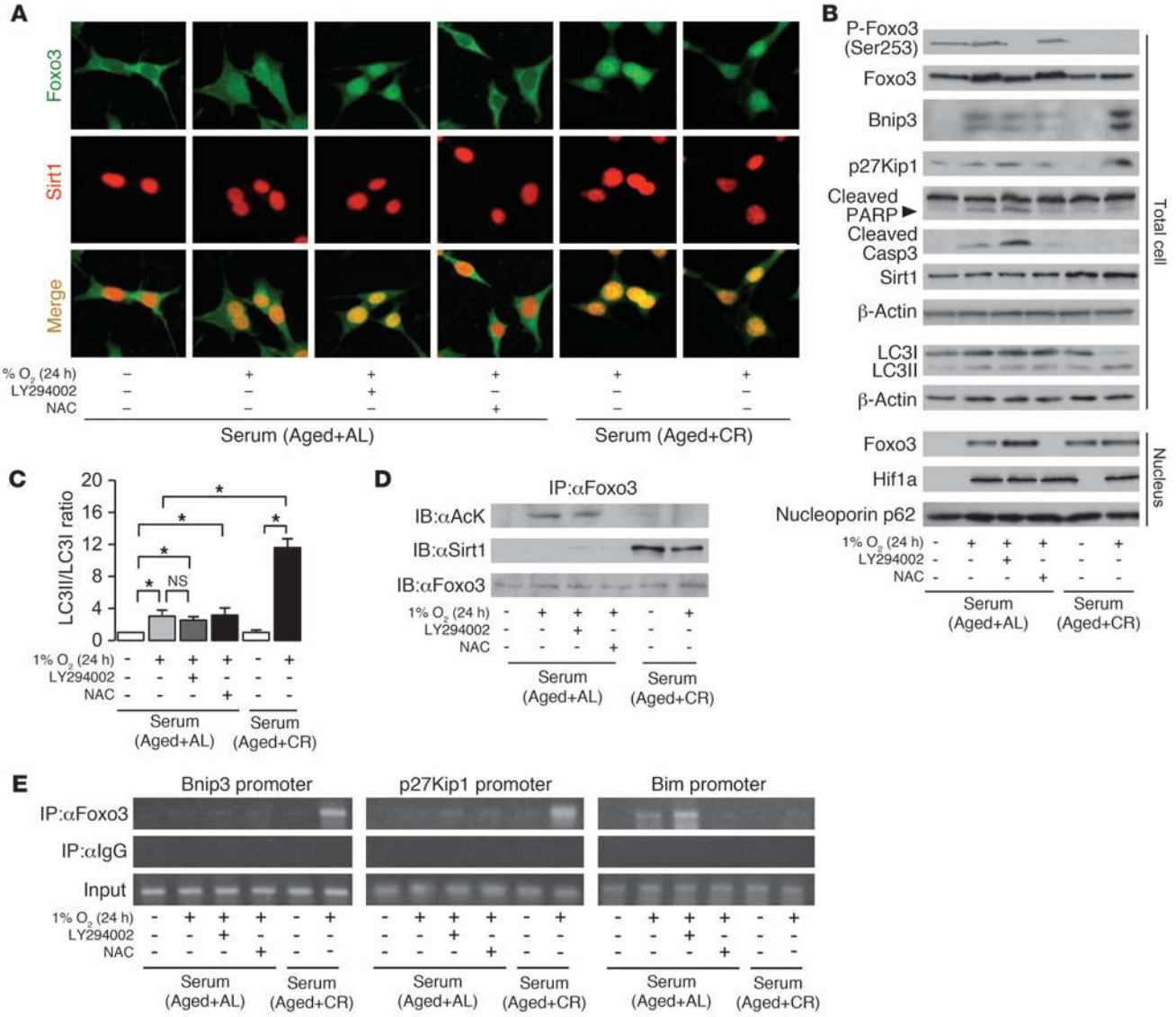

Figure 7

Involvement of PI3K and Sirt1 in Foxo3-mediated cell adaptation to hypoxia. (**A**) Immunostaining showing localization of Foxo3 and Sirt1 at late phase of hypoxia (1% O_2, 24 hours) under the indicated conditions. Original magnification, ×400. (**B**) Phosphorylation and expression level of Foxo3; expression of Bnip3, p27Kip1, cleaved PARP, cleaved caspase 3, and Sirt1; formation of LC3II; and nuclear expression levels of Foxo3 and Hif1a at late phase of hypoxia. To detect LC3I and LC3II bands, cells were preincubated with lysosomal inhibitor (E64d and pepstatin A). (**C**) Quantitative analysis of the ratio of LC3II to LC3I ($n = 4$). (**D**) Acetylation of Foxo3 and interaction between Sirt1 and Foxo3 at late phase of hypoxia. (**E**) ChIP analysis to determine Foxo3 binding to the promoters of Bnip3, p27Kip1, and Bim at late phase of hypoxia. LY294002 was used as a PI3K inhibitor at 20 μM. NAC was used as an antioxidant at 20 mM. Data are mean ± SEM. *$P < 0.05$.

decreased. CR failed to enhance hypoxia-induced Bnip3 expression and autophagy (Figure 9, D–G), which caused mitochondrial oxidative damage in the kidneys of *Sirt1*$^{+/-}$ mice (Figure 9, A–C), although they showed the systemic phenotype of CR mice (Supplemental Table 2). These results suggest that Sirt1 in the kidney is essential for the CR-mediated enhancement of hypoxia-associated mitochondria oxidative damage in vivo. We also confirmed that the phenotypes of aged kidneys of 12-month-old WT, *Sirt1*$^{+/-}$ AL, and *Sirt1*$^{+/-}$ CR mice of C57BL/6 background were similar (Supplemental Figure 2, A and B) to those of mice of SV129 background (Figure 9, A and D), which suggests that the difference in genetic background does not affect the role of Sirt1 in hypoxia-associated mitochondrial damage and cellular adaptation in the kidney.

In the kidneys of WT mice, Foxo3 interacted with Sirt1 and was deacetylated, whereas its acetylation was enhanced in *Sirt1*$^{+/-}$ mice with both AL and CR (Figure 9H). In agreement with the results of the in vitro study, deacetylated Foxo3 bound to Bnip3 and p27Kip1 promoters (Figure 9I), resulting in increased expression levels of these proteins in WT mice (Figure 9D). In contrast, acetylated Foxo3 in the kidneys of *Sirt1*$^{+/-}$ AL and CR mice failed to bind Bnip3 and p27Kip1 promoters (Figure 9I), and their expressions subsequently decreased (Figure 9D). Furthermore, Foxo3 binding to Bim pro-

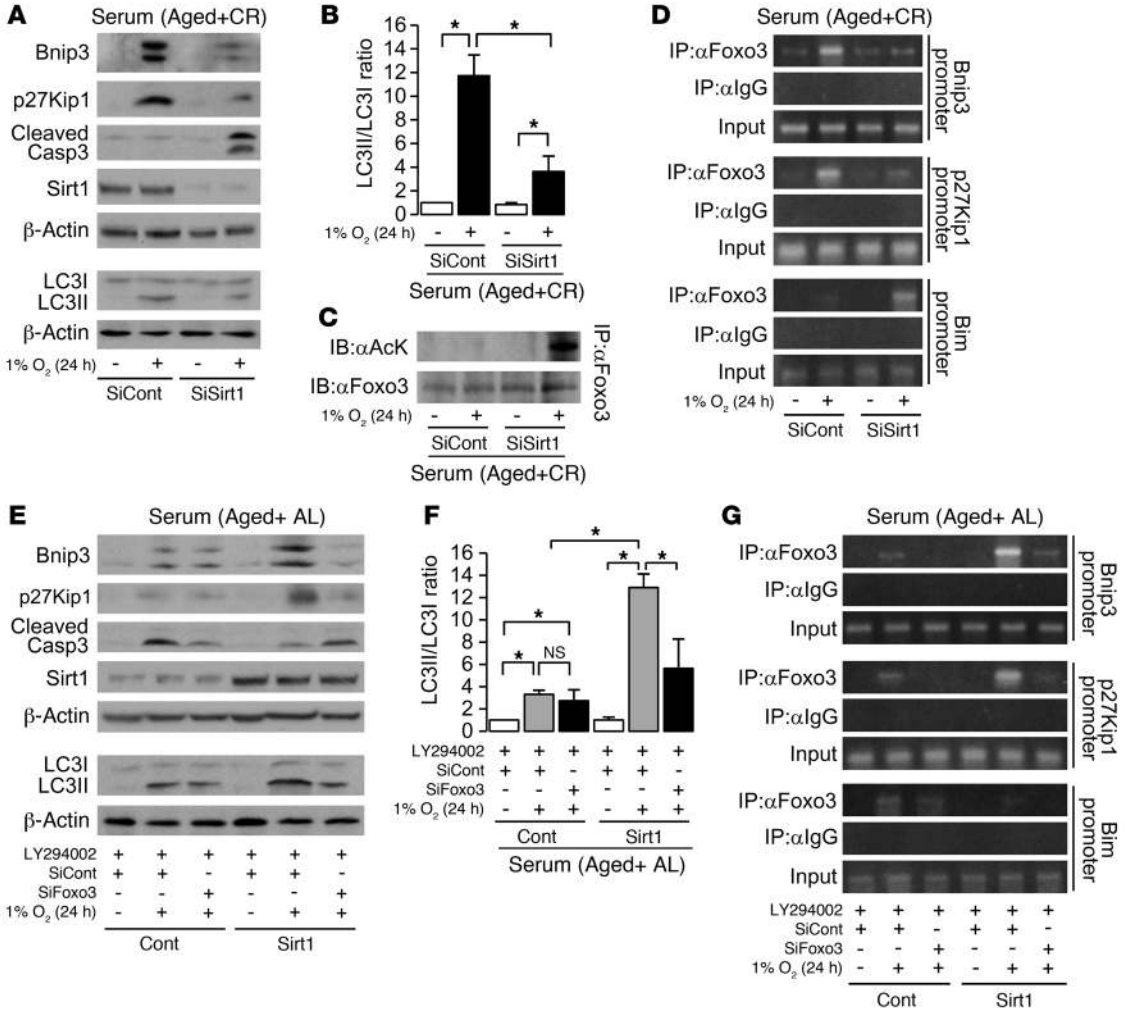

Figure 8

Role of Sirt1 in cell adaptation to hypoxia. (**A**) Expression levels of Bnip3, p27Kip1, cleaved caspase 3, and Sirt1 and formation of LC3II in retrovirally mediated Sirt1-knockdown cells under hypoxia (1% O_2, 24 hours) in CR serum condition. To detect LC3I and LC3II bands, cells were preincubated with lysosomal inhibitor (E64d and pepstatin A). (**B**) Quantitative analysis of the ratio of LC3II to LC3I ($n = 4$). (**C**) Acetylation of Foxo3 in Sirt1-knockdown cells under hypoxia in CR serum. (**D**) ChIP analysis to determine Foxo3 binding to promoters of Bnip3, p27Kip1, and Bim in Sirt1-knockdown cells under hypoxia in CR serum. (**E**) Expression levels of Bnip3, p27Kip1, cleaved caspase 3, and Sirt1 and formation of LC3II in retrovirally mediated Sirt1-overexpressing cells transfected with siRNA control or siRNA for Foxo3 under hypoxia in AL serum. To detect LC3I and LC3II bands, cells were preincubated as in **A**. (**F**) Quantitative analysis of the ratio of LC3II to LC3I ($n = 4$). (**G**) ChIP analysis to determine Foxo3 binding to promoters of Bnip3, p27Kip1, and Bim in Sirt1-overexpressing cells transfected with siRNA control or siRNA for Foxo3 under hypoxia in AL serum. LY294002 was used as a PI3K inhibitor at 20 μM. Data are mean ± SEM. $^*P < 0.05$.

moter (Figure 9I) and subsequent cleavage of caspase 3 (Figure 9D) were enhanced in the kidneys of *Sirt1*$^{+/-}$ AL and CR mice. Finally, serum cystatin C levels were significantly higher in *Sirt1*$^{+/-}$ AL mice, and were not attenuated by 6 months of CR (Figure 9J).

Discussion

Our results provided the first evidence to our knowledge that long-term CR enhances autophagy with overexpression of Sirt1 in aged tissue of mammals and is a therapeutic target for age- and hypoxia-associated tissue damage including aged kidney. In this study, we focused on Sirt1, a survival molecule under CR (23, 24, 43, 44). Recent reports suggest that *Sirt1* transgenic mice show a phenotype that resembles mice under CR (45), and *Sirt1* deficiency in mice failed to show lifespan prolongation under CR (46). However, few studies have provided direct evidence for the involvement of Sirt1 in the pathogenesis of age-associated mitochondrial damage or in the mechanism underlying long-term CR-mediated mitochondrial protection. In the present study, Sirt1 expression was significantly decreased in aged kidney and was enhanced by long-term CR. Furthermore, the results showing acetylation state of Foxo3 emphasized the suppression of Sirt1 deacetylase activity in aged kidney and its enhancement by long-term CR. We believe we are the first to show that long-term CR can cause Sirt1 activation even in aged tissues.

The in vitro model of CR has been used to determine the effects of CR serum on cell proliferation (39), apoptosis (38), and mitochondria biogenesis (20). Using this model, we showed that aging AL and CR serum affected hypoxia-induced autophagy through modification of the Sirt1-PI3K-Foxo3 axis. Sirt1 deficiency and

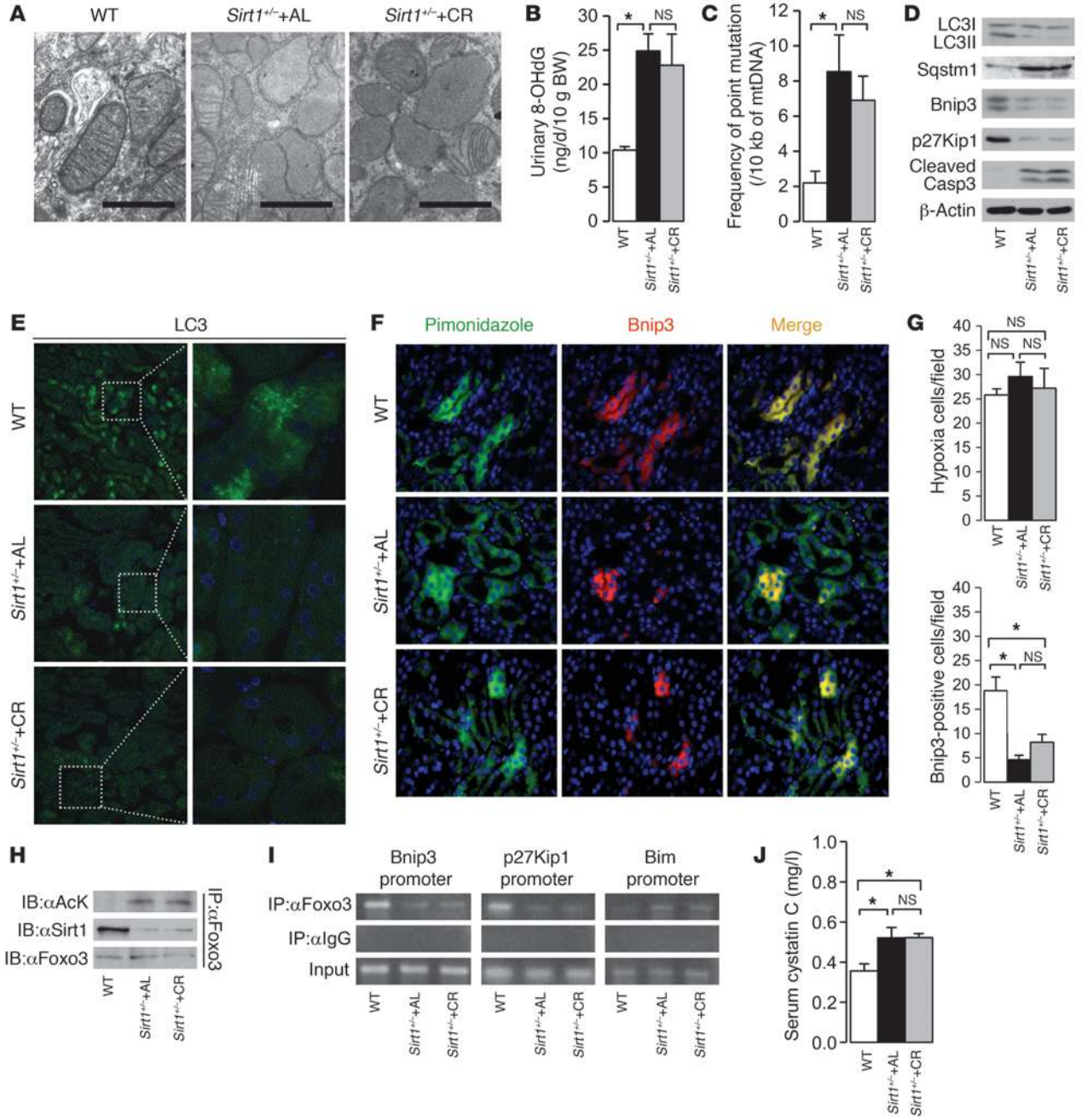

Figure 9

Effect of CR on Foxo3-mediated cell adaptation in the kidneys of aged *Sirt1*$^{+/-}$ mice. We examined 12-month-old WT mice, *Sirt1*$^{+/-}$ AL mice, and *Sirt1*$^{+/-}$ mice on CR for 6 months. (**A**) EM of a renal PTC. Scale bars: 1 μm. (**B**) Urinary 8-OHdG excretion. (**C**) Frequency of point mutation of mtDNA in the kidney. (**D**) LC3II formation and expression levels of Sqstm1, Bnip3, p27Kip1, and cleaved caspase 3 in the kidney. (**E**) Immunofluorescence study for LC3 protein in the kidney. Original magnification, ×400 (left); ×1,000 (right). (**F**) Immunofluorescence study for pimonidazole and Bnip3 in a kidney section. Original magnification, ×400. (**G**) Quantitative analysis of hypoxic pimonidazole$^+$ and Bnip3$^+$ cells per field in the kidney. (**H**) Acetylation of Foxo3 and interaction between Sirt1 and Foxo3 in the kidney. (**I**) ChIP analysis to determine Foxo3 binding to the binding site in the Bnip3, p27Kip1, and Bim promoters in the kidney. (**J**) Serum cystatin C levels at the end of experimental periods. Data are mean ± SEM. *$P < 0.05$. Each group includes 5–7 mice.

enhanced PI3K during the aging process suppress both autophagy and cell cycle arrest even under hypoxic conditions, which results in accumulation of oxidative stress and subsequent apoptosis through acetylated Foxo3-mediated Bim expression (Figure 10A). In contrast, CR-mediated Sirt1 activation promotes cell adaptation to hypoxia through Bnip3-mediated autophagy and p27Kip1 expression via deacetylation of Foxo3 (Figure 10B). Furthermore, the results of in vivo study showing the effect of CR on age-associated kidney phenotypes in *Sirt1*$^{+/-}$ mice were in agreement with this molecular mechanism. Our present results provide insight into the molecu-

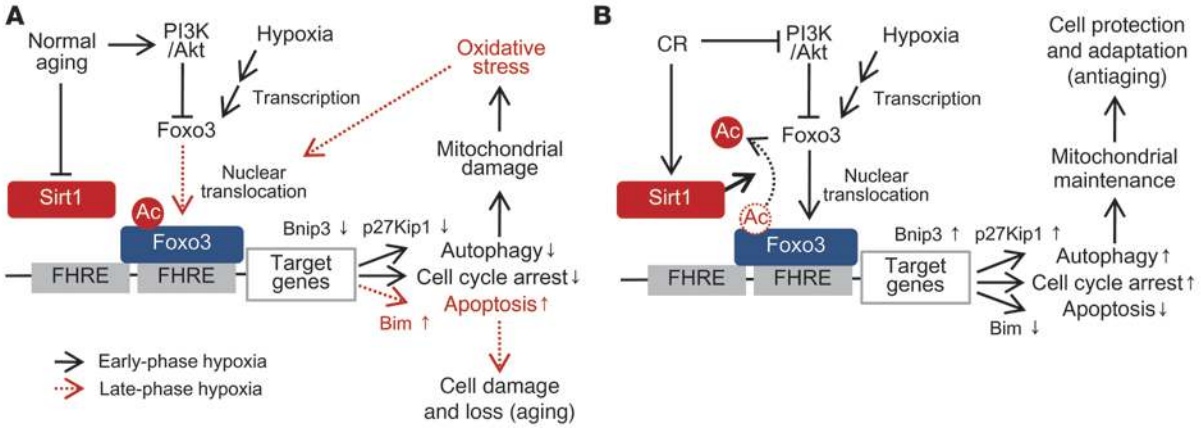

Figure 10

Molecular mechanisms underlying CR-mediated cellular adaptation to hypoxia in aged kidney. (**A**) The normal aging process inhibits Sirt1 activity. During early-stage hypoxia, hypoxia fails to enhance nuclear translocation of Foxo3, subsequent autophagy, and cell cycle arrest, which increases mitochondrial oxidative damage (black lines). At late-phase hypoxia, hypoxia-associated oxidative stress activates nuclear translocation of acetylated Foxo3, which promotes apoptosis (red lines). (**B**) CR activates Sirt1 activity and nuclear translocation of Foxo3, which promotes autophagy and cell cycle arrest under hypoxia to maintain normal mitochondria function under hypoxia.

lar mechanism of CR-mediated cell adaptation to age-associated hypoxia. Because stress-induced apoptosis and cell loss have been implicated in age-associated diseases (47), Sirt1 deficiency–mediated apoptosis should be involved in age-dependent kidney dysfunction through loss of PTCs, and Sirt1-mediated cell adaptation to hypoxia is essential for the CR-mediated kidney protection.

A recent study reported that Sirt1 regulates autophagy through deacetylation of certain molecules associated with autophagy under starvation, but not hypoxia (48). However, how the autophagic machinery selectively destroys damaged mitochondria remains elusive. A study showed that Bnip3 selectively and positively regulates hypoxia-induced mitochondrial autophagy through the disruption of bcl2-beclin1 interaction (15), suggesting that Sirt1-Foxo3 pathway–mediated Bnip3 overexpression may be the regulatory mechanism through which the autophagic machinery selectively destroys damaged mitochondria under hypoxia.

Nuclear translocation of Foxo3 is negatively regulated by PI3K-Akt–mediated phosphorylation (40) and positively by oxidative stress (37, 49). Under AL serum, phosphorylated Foxo3 showed cytoplasmic distribution at the early phase of hypoxia, which suppressed hypoxia-induced autophagy and increased oxidative stress. In contrast, during the late phase of hypoxia under AL serum, Foxo3 translocated into the nucleus in response to oxidative stress, resulting in Foxo3-mediated apoptosis through Bim expression, and this process was enhanced by PI3K inhibition. Thus, under hypoxia in AL serum, the PI3K-Akt pathway plays a biphasic role, increasing mitochondrial oxidative stress through inhibition of autophagy and suppressing Foxo3-mediated apoptosis under oxidative stress. These findings are in agreement with the notion that acceleration of the insulin-PI3K-Akt pathway enhances the aging process (50), but has an antiapoptotic effect against hypoxia (51) and oxidative stress (40). Furthermore, Sirt1 attenuated PI3K inhibition–mediated acceleration of apoptosis under AL serum, which suggests that Sirt1, rather than PI3K, plays a central role for cell survival in the aging process.

Foxo3 promotes resistance to certain stress (37, 52), whereas it promotes apoptosis under other stress (40). However, how Foxo3 selects the exact target gene in response to a specific condition remains obscure. In this study, under CR serum, Foxo3 was deacetylated by Sirt1 and bound to p27Kip1 and Bnip3 promoter, resulting in cell adaptation to hypoxia. In contrast, acetylated Foxo3 enhanced hypoxia-related apoptosis through Bim overexpression under AL serum. A prior report suggested that Sirt1 regulates Foxo3 transcriptional activity under oxidative stress to promote cell survival (37). In addition to this, our results provide further evidence that Sirt1-mediated deacetylation of Foxo3 is essential for cell survival and the mechanism by which Foxo3 selects a specific gene promoter.

The present study demonstrated that mitochondrial damage in aged kidney is associated with Sirt1 deficiency and that Sirt1 promotes cell adaptation to hypoxia through autophagy in aged kidney. Our results provide what we believe to be the first evidence that Sirt1, the PI3K-Akt pathway, and Foxo3 coordinately regulate age-dependent tissue dysfunction and autophagy in mammals, as previously reported in lower organisms (23, 24, 53, 54). The reduced autophagy in the kidney may be involved in the age-associated weakness of PTCs against various renal toxicities, such as drug toxicity and proteinuria in glomerular diseases. Autophagy is currently the focus of research in various fields, such as aging (55), metabolic diseases (56, 57), and immune diseases (58). Our concept should be helpful in the design of studies aiming to further explore autophagy-related diseases and lead to the establishment of new therapies that can delay the progression of hypoxia- and age-related tissue dysfunction, including CKD in elderly patients.

Methods

Study approval. The Research Center for Animal Life Science of Shiga University of Medical Science approved all animal experiments.

Reagents and materials. Anti-LC3 and anti-Hif1a were purchased from NOVUS Biologicals. Anti-Sqstm1/p62 was from Progen. Anti–nucleoporine p62 was from BD Biosciences. Anti-beclin1, anti-p27Kip1, and anti-Bcl2 was from Santa Cruz Biotechnology Inc. Anti-Sirt1 was from Upstate Cell Signaling. Anti-GAPDH was from Chemicon. Anti-Bnip3, anti-pFoxo3 (Ser253), anti-Foxo3, anti–cleaved caspase 3, anti-PARP, and anti-acetyllysine were from Cell Signaling Technology. Anti-8OHdG was from Japan

Institute for the Control of Aging. Hypoxyprobe-1 kit was obtained from Natural Pharmacia International Inc. Anti–β-actin, E64d, pepstatin A, LY294002, and NAC were from Sigma-Aldrich.

CR in aged mice. Experiments were performed essentially as described previously (59). Male C57BL/6 mice were obtained from CLEA Japan. Six-week-old mice were maintained on a 12-hour light/12-hour dark cycle and provided food and water AL for 12 months. At 12 months of age, they were divided into 2 groups: AL and CR (n = 10 per group). During the following 12 months, mice of the CR group were fed an amount of food corresponding to 60% of the amount of food consumed by the AL group. Food consumption was measured every 2 weeks, and the results were used to calculate the daily food intake. Finally, the 24-month-old (aged) AL and CR mice and the 3-month-old (young) mice were sacrificed (60).

CR in Sirt1$^{+/-}$ mice. The *Sirt1*$^{-/-}$ mouse strain on SV129 background were provided by F.W. Alt (Harvard University, Boston, Massachusetts; ref. 61). Male *Sirt1*$^{+/-}$ mice and their WT littermates were provided food and water AL for 6 months. At 6 months of age, they were divided into 3 groups — WT mice with AL (n = 6), *Sirt1*$^{+/-}$ mice with AL (n = 10), and *Sirt1*$^{+/-}$ mice with CR (n = 10) — and followed for the next 6 months. During the 6-month observation period, 1 WT mouse, 3 *Sirt1*$^{+/-}$ mice with AL, and 3 *Sirt1*$^{+/-}$ mice with CR died from neoplasia. Finally, at 12 months of age, we sacrificed 5 WT control mice, 7 *Sirt1*$^{+/-}$ AL mice, and 7 *Sirt1*$^{+/-}$ CR mice.

Serum cystatin C and urinary albumin level. Serum cystatin C was determined using Cystatin C (mouse) ELISA Kit (ALEXIS Biochemicals). Urinary albumin excretion was measured with a mouse-specific sandwich ELISA system (Albuwell; Exocell) and was expressed as the total amount excreted in 24 hours (60).

Histopathological examination. For semiquantitative evaluation of the fibrotic and 8-OHdG scores, 20 randomly selected glomerulus or tubulointerstitial areas per mouse were graded in a double-blind manner, as reported previously (60), with minor modifications.

Quantitative RT-PCR. Isolation of total RNA from kidney, and determination of cDNA synthesis by reverse transcription and quantitative real-time PCR were performed as described previously (60). The sequences of the primers are provided in Supplemental Table 3.

EM. Parts of the removed kidneys were cut into small tissue blocks (1 mm^3), and fixed in 2.0% glutaraldehyde and 2.0% paraformaldehyde with 0.1 mol/l phosphate buffer at 4°C. After fixation with 2% osmium tetroxide, tissues were dehydrated in a series of graded ethanol solutions, ethanol was substituted with propylene oxide, and then embedded in epoxy resin. Ultrathin sections were double-stained with uranyl acetate and lead. Sections were examined under a JEM1200EX EM (JOEL) at 80 kV.

Cells. Mouse renal PTCs were cultured as described previously (62). Sera from aged AL and CR rats (60% of AL for 12 months) were obtained and used as described previously (20, 38, 39). After 24 hours of starvation with serum-free DMEM, the cultured PTCs grown in the presence of serum from CR or AL animals for 6 hours were exposed to hypoxia (1% O_2) under the indicated conditions.

Transient transfection of siRNA. siRNA for control and siRNA for Foxo3 were purchased from Ambion. Transient transfection of siRNA was performed using Lipofectamine 2000 (Invitrogen) (63). Hypoxic studies were performed after 24 hours of siRNA transfection.

Plasmids and viral infection. For the production of retrovirus, full-length cDNA of mouse *Bnip3* was amplified by PCR, subcloned into pCR-TOPO II vectors (Invitrogen), and inserted into pBABE vectors. pBABE-Sirt1, pSUPER-siSirt1, and pSUPER-siBnip3 were provided by L. Guarente (Massachusetts Institute of Technology, Cambridge; ref. 64) and by K. Inoki (University of Michigan, Ann Arbor). The indicated retrovirus vectors were generated and infected into cells as reported previously (63). Adenovirus for Sirt1 was provided by T. Kitamura and T. Sasaki (Gunma University, Maebashi, Japan).

IP and IB. Homogenates of whole kidney and PTCs in lysis buffer containing nicotinamide were mixed with Foxo3 antibody and followed by the addition of protein A/G–Sepharose. IP and IB were performed as described previously (63).

In vitro autophagy assays. Autophagy was visualized in cultured PTCs by transfection of GFP-LC3 (cDNA of LC3 was provided by T. Yoshimori, Osaka University, Japan, and N. Mizushima, Tokyo Medical and Dental University, Japan; refs. 32, 33). To detect autophagy by Western blot analysis, the indicated cells were treated with E64d and pepstatin A to inhibit lysosomal enzyme activity (33).

ChIP assay. The ChIP experiments on kidney samples or PTCs were performed using the ChIP-IT kit from Active Motif according to the instructions provided by the manufacturer. Primer sequences are listed in Supplemental Table 3.

Immunofluorescent study. To detect hypoxic conditions in each group of mice, a chemical probe for hypoxia, pimonidazole (Belmont), was injected intraperitoneally 1 hour before sacrifice. For immunofluorescence staining, we incubated frozen kidney sections with antibodies against pimonidazole and Bnip3 or LC3. The cultured PTCs were fixed with acetone for 10 minutes and incubated with antibodies against Sirt1 and Foxo3 after blocking with 2% BSA in PBS, using the protocols described previously (63).

8-OHdG levels, point mutation, and deletion mutation in mtDNA. The mtDNA was extracted from the kidney using the mtDNA Extractor CT kit (Wako). The 8-OHdG levels in DNase I–digested mtDNA were determined by ELISA (Japan Institute for the Control of Aging; ref. 65). To determine the sequence of cytochrome *b* gene in mtDNA, we amplified its coding region with Pfu-ultra polymerase (Invitrogen) using the primers listed in Supplemental Table 3. The PCR-amplified fragments were subcloned into TOPO TA cloning kit (Invitrogen) and sequenced with the M13 primer (65). We assayed a common deletion mutation, D-17 (28), in mtDNA using quantitative PCR with primers flanking the D-17 deletion and with template mtDNAs cut at an *Mlu*I site present in the region deleted in D-17 (65). The sequences of primers for the normal and D-17–deleted cytochrome *b* gene are provided in Supplemental Table 3.

NAD content. NAD content was determined using the NAD/NADH Quantitation Kit (BioVision) and the protocol supplied by the manufacturer.

Statistics. All values are expressed as mean ± SEM. Differences among multiple data sets were analyzed by 1- or 2-way ANOVA, followed by Scheffé's test. Statistical analyses of correlations were performed with the JMP program (version 5.0; SAS Institute Japan). The distribution of variables was analyzed by checking the data histograms, and normal distribution was tested by the Kolmogorov-Smirnov and Shapiro-Wilk tests. Pearson correlation coefficients were calculated to investigate the association among the indicated parameters. In all analyses, a P value less than 0.05 denoted the presence of a statistically significant difference.

Acknowledgments

We thank L. Guarente (Massachusetts Institute of Technology, Cambridge) and K. Inoki (University of Michigan, Ann Arbor) for helpful discussions and providing materials and H. Inoue, T. Yoshizaki, and M. Sera (Shiga University of Medical Science) and the Central Research Laboratory of Shiga University of Medical Science for valuable technical assistance. We also thank T. Kitamura and T. Sasaki (Gunma University, Japan), T. Yoshimori (Osaka University, Japan), and N. Mizushima (Tokyo Medical and Dental University, Japan) for providing materials and Frederick W. Alt (Harvard University, Cambridge) and S. Ezoe (Osaka University) for the *Sirt1*$^{-/-}$ mouse strain. S. Kume is a Research Fellow of the Japan Society for the Promotion of Science (JSPS). This study was supported by a Grant-in-Aid for JSPS Fellows to S. Kume, Grants-

in-Aid for Scientific Research to D. Koya, and a grant from the Uehara Memorial Foundation to D. Koya.
Received for publication October 8, 2009, and accepted in revised form January 20, 2010.

Address correspondence to: Daisuke Koya, Division of Endocrinology and Metabolism, Kanazawa Medical University, Uchinada-Cho, Kahoku-Gun, Ishikawa 920-0293, Japan. Phone: 81.76.286.2211; Fax: 81.76.286.6927; E-mail: koya0516@kanazawa-med.ac.jp.

1. Baylis C, Corman B. The aging kidney: insights from experimental studies. *J Am Soc Nephrol*. 1998; 9(4):699–709.
2. Coresh J, Astor BC, Greene T, Eknoyan G, Levey AS. Prevalence of chronic kidney disease and decreased kidney function in the adult US population: Third National Health and Nutrition Examination Survey. *Am J Kidney Dis*. 2003;41(1):1–12.
3. Epstein M. Aging and the kidney. *J Am Soc Nephrol*. 1996;7(8):1106–1122.
4. Cutler RG. Human longevity and aging: possible role of reactive oxygen species. *Ann N Y Acad Sci*. 1991; 621:1–28.
5. Droge W. Free radicals in the physiological control of cell function. *Physiol Rev*. 2002;82(1):47–95.
6. Hutter E, Unterluggauer H, Garedew A, Jansen-Durr P, Gnaiger E. High-resolution respirometry--a modern tool in aging research. *Exp Gerontol*. 2006; 41(1):103–109.
7. Yowe DL, Ames BN. Quantitation of age-related mitochondrial DNA deletions in rat tissues shows that their pattern of accumulation differs from that of humans. *Gene*. 1998;209(1–2):23–30.
8. Inoue S, Ishikawa K, Nakada K, Sato A, Miyoshi H, Hayashi J. Suppression of disease phenotypes of adult mito-mice carrying pathogenic mtDNA by bone marrow transplantation. *Hum Mol Genet*. 2006;15(11):1801–1807.
9. Rotig A. Renal disease and mitochondrial genetics. *J Nephrol*. 2003;16(2):286–292.
10. Nohl H, Staniek K, Gille L. Imbalance of oxygen activation and energy metabolism as a consequence or mediator of aging. *Exp Gerontol*. 1997; 32(4–5):485–500.
11. Roberts EL Jr, Chih CP, Rosenthal M. Age-related changes in brain metabolism and vulnerability to anoxia. *Adv Exp Med Biol*. 1997;411:83–89.
12. Pepe S. Mitochondrial function in ischaemia and reperfusion of the ageing heart. *Clin Exp Pharmacol Physiol*. 2000;27(9):745–750.
13. Nangaku M, Inagi R, Miyata T, Fujita T. Hypoxia and hypoxia-inducible factor in renal disease. *Nephron Exp Nephrol*. 2008;110(1):e1–e7.
14. Chandel NS, Budinger GR. The cellular basis for diverse responses to oxygen. *Free Radic Biol Med*. 2007;42(2):165–174.
15. Zhang H, et al. Mitochondrial autophagy is an HIF-1-dependent adaptive metabolic response to hypoxia. *J Biol Chem*. 2008;283(16):10892–10903.
16. Kim H, Lee DK, Choi JW, Kim JS, Park SC, Youn HD. Analysis of the effect of aging on the response to hypoxia by cDNA microarray. *Mech Ageing Dev*. 2003;124(8–9):941–949.
17. Serebrovskaya TV, et al. Geriatric men at altitude: hypoxic ventilatory sensitivity and blood dopamine changes. *Respiration*. 2000;67(3):253–260.
18. Masoro EJ. Caloric restriction and aging: an update. *Exp Gerontol*. 2000;35(3):299–305.
19. Weindruch R, Sohal RS. Seminars in medicine of the Beth Israel Deaconess Medical Center. Caloric intake and aging. *N Engl J Med*. 1997;337(14):986–994.
20. Lopez-Lluch G, et al. Calorie restriction induces mitochondrial biogenesis and bioenergetic efficiency. *Proc Natl Acad Sci U S A*. 2006;103(6):1768–1773.
21. McKiernan SH, et al. Adult-onset calorie restriction delays the accumulation of mitochondrial enzyme abnormalities in aging rat kidney tubular epithelial cells. *Am J Physiol Renal Physiol*. 2007; 292(6):F1751–F1760.
22. Kim HJ, Jung KJ, Yu BP, Cho CG, Choi JS, Chung HY. Modulation of redox-sensitive transcription factors by calorie restriction during aging. *Mech Ageing Dev*. 2002;123(12):1589–1595.
23. Kaeberlein M, Andalis AA, Fink GR, Guarente L. High osmolarity extends life span in Saccharomyces cerevisiae by a mechanism related to calorie restriction. *Mol Cell Biol*. 2002;22(22):8056–8066.
24. Lin SJ, Defossez PA, Guarente L. Requirement of NAD and SIR2 for life-span extension by calorie restriction in Saccharomyces cerevisiae. *Science*. 2000; 289(5487):2126–2128.
25. Guarente L, Picard F. Calorie restriction--the SIR2 connection. *Cell*. 2005;120(4):473–482.
26. Michan S, Sinclair D. Sirtuins in mammals: insights into their biological function. *Biochem J*. 2007; 404(1):1–13.
27. Michikawa Y, Mazzucchelli F, Bresolin N, Scarlato G, Attardi G. Aging-dependent large accumulation of point mutations in the human mtDNA control region for replication. *Science*. 1999; 286(5440):774–779.
28. Tanhauser SM, Laipis PJ. Multiple deletions are detectable in mitochondrial DNA of aging mice. *J Biol Chem*. 1995;270(42):24769–24775.
29. Mizushima N. Autophagy: process and function. *Genes Dev*. 2007;21(22):2861–2873.
30. Bjorkoy G, et al. p62/SQSTM1 forms protein aggregates degraded by autophagy and has a protective effect on huntingtin-induced cell death. *J Cell Biol*. 2005;171(4):603–614.
31. Nakai A, et al. The role of autophagy in cardiomyocytes in the basal state and in response to hemodynamic stress. *Nat Med*. 2007;13(5):619–624.
32. Kabeya Y, et al. LC3, a mammalian homologue of yeast Apg8p, is localized in autophagosome membranes after processing. *EMBO J*. 2000;19(21):5720–5728.
33. Klionsky DJ, et al. Guidelines for the use and interpretation of assays for monitoring autophagy in higher eukaryotes. *Autophagy*. 2008;4(2):151–175.
34. Hamacher-Brady A, et al. Response to myocardial ischemia/reperfusion injury involves Bnip3 and autophagy. *Cell Death Differ*. 2007;14(1):146–157.
35. Tracy K, et al. BNIP3 is an RB/E2F target gene required for hypoxia-induced autophagy. *Mol Cell Biol*. 2007;27(17):6229–6242.
36. Mammucari C, et al. FoxO3 controls autophagy in skeletal muscle in vivo. *Cell Metab*. 2007; 6(6):458–471.
37. Brunet A, et al. Stress-dependent regulation of FOXO transcription factors by the SIRT1 deacetylase. *Science*. 2004;303(5666):2011–2015.
38. Cohen HY, et al. Calorie restriction promotes mammalian cell survival by inducing the SIRT1 deacetylase. *Science*. 2004;305(5682):390–392.
39. de Cabo R, Furer-Galban S, Anson RM, Gilman C, Gorospe M, Lane MA. An in vitro model of caloric restriction. *Exp Gerontol*. 2003;38(6):631–639.
40. Brunet A, et al. Akt promotes cell survival by phosphorylating and inhibiting a Forkhead transcription factor. *Cell*. 1999;96(6):857–868.
41. Medema RH, Kops GJ, Bos JL, Burgering BM. AFX-like Forkhead transcription factors mediate cell-cycle regulation by Ras and PKB through p27kip1. *Nature*. 2000;404(6779):782–787.
42. Essafi A, et al. Direct transcriptional regulation of Bim by FoxO3a mediates STI571-induced apoptosis in Bcr-Abl-expressing cells. *Oncogene*. 2005; 24(14):2317–2329.
43. Anderson RM, Bitterman KJ, Wood JG, Medvedik O, Sinclair DA. Nicotinamide and PNC1 govern lifespan extension by calorie restriction in Saccharomyces cerevisiae. *Nature*. 2003;423(6936):181–185.
44. Lin SJ, Ford E, Haigis M, Liszt G, Guarente L. Calorie restriction extends yeast life span by lowering the level of NADH. *Genes Dev*. 2004;18(1):12–16.
45. Bordone L, et al. SIRT1 transgenic mice show phenotypes resembling calorie restriction. *Aging Cell*. 2007;6(6):759–767.
46. Boily G, et al. SirT1 regulates energy metabolism and response to caloric restriction in mice. *PLoS One*. 2008;3(3):e1759.
47. Higami Y, Shimokawa I. Apoptosis in the aging process. *Cell Tissue Res*. 2000;301(1):125–132.
48. Lee IH, et al. A role for the NAD-dependent deacetylase Sirt1 in the regulation of autophagy. *Proc Natl Acad Sci U S A*. 2008;105(9):3374–3379.
49. Marinkovic D, et al. Foxo3 is required for the regulation of oxidative stress in erythropoiesis. *J Clin Invest*. 2007;117(8):2133–2144.
50. Bartke A. Insulin and aging. *Cell Cycle*. 2008; 7(21):3338–3343.
51. Brunelle JK, Chandel NS. Oxygen deprivation induced cell death: an update. *Apoptosis*. 2002;7(6):475–482.
52. Mei Y, Zhang Y, Yamamoto K, Xie W, Mak TW, You H. FOXO3a-dependent regulation of Pink1 (Park6) mediates survival signaling in response to cytokine deprivation. *Proc Natl Acad Sci U S A*. 2009; 106(13):5153–5158.
53. Ogg S, et al. The Fork head transcription factor DAF-16 transduces insulin-like metabolic and longevity signals in *C. elegans*. *Nature*. 1997;389(6654):994–999.
54. Sigmond T, et al. Autophagy in *Caenorhabditis elegans*. *Methods Enzymol*. 2008;451:521–540.
55. Zhang C, Cuervo AM. Restoration of chaperone-mediated autophagy in aging liver improves cellular maintenance and hepatic function. *Nat Med*. 2008;14(9):959–965.
56. Ebato C, et al. Autophagy is important in islet homeostasis and compensatory increase of beta cell mass in response to high-fat diet. *Cell Metab*. 2008;8(4):325–332.
57. Singh R, et al. Autophagy regulates lipid metabolism. *Nature*. 2009;458(7242):1131–1135.
58. Sanjuan MA, et al. Toll-like receptor signalling in macrophages links the autophagy pathway to phagocytosis. *Nature*. 2007;450(7173):1253–1257.
59. Piper MD, Bartke A. Diet and aging. *Cell Metab*. 2008;8(2):99–104.
60. Kume S, et al. Role of altered renal lipid metabolism in the development of renal injury induced by a high-fat diet. *J Am Soc Nephrol*. 2007;18(10):2715–2723.
61. Cheng HL, et al. Developmental defects and p53 hyperacetylation in Sir2 homolog (SIRT1)-deficient mice. *Proc Natl Acad Sci U S A*. 2003; 100(19):10794–10799.
62. Takaya K, et al. Involvement of ERK pathway in albumin-induced MCP-1 expression in mouse proximal tubular cells. *Am J Physiol Renal Physiol*. 2003; 284(5):F1037–F1045.
63. Kume S, et al. SIRT1 inhibits transforming growth factor beta-induced apoptosis in glomerular mesangial cells via Smad7 deacetylation. *J Biol Chem*. 2007;282(1):151–158.
64. Picard F, et al. Sirt1 promotes fat mobilization in white adipocytes by repressing PPAR-gamma. *Nature*. 2004;429(6993):771–776.
65. Kakoki M, et al. Senescence-associated phenotypes in Akita diabetic mice are enhanced by absence of bradykinin B2 receptors. *J Clin Invest*. 2006; 116(5):1302–1309.